Direct numerical simulation of a mixing layer downstream a thick splitter plate

Sylvain Laizet,[1,2,a)] Sylvain Lardeau,[1] and Eric Lamballais[2]

[1]*Department of Aeronautics, Imperial College London, London SW7 2AZ, United Kingdom*
[2]*Laboratoire d'Etudes Aérodynamiques UMR 6609, Université de Poitiers, CNRS Téléport 2,*
Bd. Marie et Pierre Curie, BP 179, 86962 Futuroscope Chasseneuil Cedex, France

In this numerical study, the flow obtained behind a trailing edge separating two streams of different velocities is studied by means of direct numerical simulation. The main originality of this work is that the splitter plate itself is included in the computational domain using an immersed boundary method. The influence of the trailing-edge shape is considered through the analysis of the destabilizing mechanisms and their resulting effect on the spatial development of the flow. The streamwise evolution of the different flows is found to be very different for each of the configurations considered, both in terms of mean quantities and flow dynamics. Present results suggest that the wake component, which dominates the flow close to the trailing edge, is still influential further downstream, as already observed in pure wake flows but only conjectured in mixing layer. A detailed analysis of the vortex dynamics is proposed using instantaneous visualizations, statistical/stability analysis considerations, and proper orthogonal decomposition in order to better understand how the transition regime from the wake to the mixing layer occurs and why it can influence the self-similarity, in a region where no wake influence can be locally detected. © *2010 American Institute of Physics.* [doi:10.1063/1.3275845]

I. INTRODUCTION

It is well known that the spatial or temporal development of turbulent wakes or mixing layers is strongly influenced by the dynamics of large-scale structures. In a wake flow, the alternating large vortices (called von Kàrmàn vortices) are initially created through a vortex shedding mechanism occurring immediately behind the body considered. In a mixing layer, the formation of primary structures leads to corotating Kelvin–Helmholtz vortices. In terms of stability, the mechanisms responsible for the growth and formation of those structures are of different nature. In typical wake flows, the vortex shedding is a self-excited phenomenon that can be interpreted in terms of global instability.[1,2] Furthermore, another well-known property of wake flows is their self-similar dependence on the inflow (generation) conditions. For instance, the spreading rate of a turbulent wake behind a plate differs from the one behind a cylinder, as well as other turbulent statistics such as velocity fluctuations. This ability of a wake to keep the memory of its generation, even in turbulent self-similar state, is discussed in Ref. 3. In addition, Kelvin–Helmholtz formation in spatially developing mixing layer admits a strong sensitivity to upstream conditions,[4] as a consequence of the convectively unstable character of this type of flow.

Most of the numerical investigations of free shear layers are based on temporal simulations, with an initial mixing-layer profile given by a hyperbolic tangent function. However, this assumption has been challenged recently since important discrepancies between experiments conducted at similar Reynolds number have been observed, e.g., Refs. 5–7. The most representative examples of these discrepancies are the origin and the role of the large spanwise structures first described in Ref. 8 that cannot be clearly understood or even reproduced in temporal simulations[6] in a context of fully developed turbulence. Furthermore, none of the temporal simulations is able to take into account the presence of the splitter plate in the experiments. In Ref. 9 it was shown that the splitter plate wake plays a very dominant role in the development of the flow and strongly interacts with the mixing layer.

In some cases, the flow over a given geometry can lead to an asymmetric wake that can be viewed as a flow with a double component wake/mixing layer. Compared to a conventional wake configuration, a breaking in the symmetry can deeply modify the spatial development of the flow. In the same way, a wake component introduced in a pure mixing layer is able to generate different mechanisms in the vortex generation behind the geometry. In order to investigate the dynamics of this type of hybrid flow, we consider in this numerical study the general flow configuration where two independent streams of velocities U_1 and U_2 (where U_1 is the high-speed velocity and U_2 is the low-speed velocity) flow on opposite sides of a semi-infinite thick trailing edge for different shapes.

Very few direct numerical simulations of spatially developing mixing layers have been published. The formation of three-dimensional (3D) vortices in spatially growing incompressible mixing layers by means of large eddy simulation (LES) was studied in Ref. 10 and some comparisons with previous temporal simulations were made. Very large direct

---

a)Author to whom correspondence should be addressed. Electronic mail:
s.laizet@imperial.ac.uk.

numerical simulation (DNS) of a spatially developing mixing layer was performed in Ref. 11, using a hyperbolic tangent profile at the inlet, in order to investigate the relationship between characteristics of the coherent fine-scale eddies and the laminar-turbulent transition. In both studies, the inlet mixing-layer velocity profile is prescribed using a hyperbolic tangent without any modeling of the wake component introduced by the splitter plate.

The importance of trailing edge has transpired in very few studies and only recently has there been a regain of interest in studying the early flow development of turbulent and transitional mixing layers. The early development of a turbulent mixing layer downstream of a splitter plate with zero thickness between a turbulent and a laminar boundary layer was investigated in Ref. 7. The geometry of the splitter plate itself is another factor which can be of importance in the spatial development of free shear layers. Indeed, the authors of Ref. 5 observed in their recent temporal simulations the absence of large-scale spanwise structures. The authors of Refs. 7 and 12–14 showed that the flow structure close to the trailing edge is primarily influenced by the geometry of the splitter plate and can deeply influence the streamwise evolution of the flow. It is important to notice that most of the stability analyses have eluded this particular aspect, except few studies such as Refs. 15 and 16. The influence of the ratio between the boundary layer thicknesses and the splitter plate, for a wide range of flow conditions, was studied experimentally in Ref. 17. Their main conclusion is that the spreading rate decreases with this ratio and that the self-similar region is shifted downstream as the trailing-edge thickness increases. They also showed that classical theories are insufficient to explain the behavior of this type of mixing layer. However, they did not focus on the near trailing-edge region and did not relate this conclusion to any particular flow structures,[15] and later the authors of Ref. 16 were among the first to study the stability of asymmetric wakes. In particular, they investigated the domain of absolute and convective instability for a family of plane wake-shear layer velocity profiles.

In this paper, following these previous studies, three different geometries of splitter plate trailing edge are considered, two of them are related to the experimental setup in Ref. 14. The main purpose of this numerical work is to investigate the role of the geometry of the splitter plate and its related wake effect on the flow dynamic downstream the trailing edge. As in Ref. 13, the modeling of the upstream condition is accurately ensured in the computation by an immersed boundary method (IBM) in order to take into account the wake effect behind the thick trailing edge. This approach has already been successfully used to simulate different types of flow in presence of various body geometries.[18–21]

The organization of this paper is as follows. Section II presents the physical configuration, its numerical modeling, and the basis of the proper orthogonal decomposition (POD) method used in this study. Section III deals with the flow dynamics in the region close to the trailing edge where instantaneous visualizations, statistical, stability, and POD analyses are presented. Then, investigations of the flow dy-
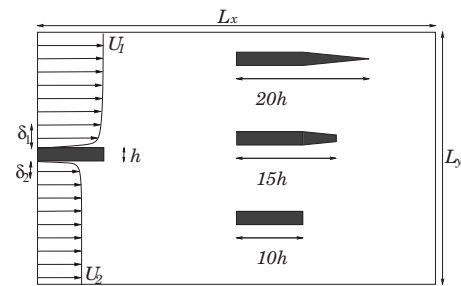

FIG. 1. Flow configuration and computational domain for the TTE (top, simulation TTE), the ITE (middle, simulation ITE), and the BTE (bottom, simulation BTE).

namics in the region further downstream are carried out in Sec. IV, through instantaneous visualizations, statistical, and POD analyses. Finally, the main results of this study are discussed in Sec. V.

II. FLOW PARAMETERS AND NUMERICAL MODELING

A. Physical and numerical parameters

In this numerical study, three different splitter plate geometries are investigated: a blunt trailing edge (BTE) of constant thickness h, a more conventional thin trailing edge (TTE) (with a bevel added to the BTE), and an intermediate trailing edge (called ITE), which ends with a thickness of $h/2$, using only half the bevel of the TTE case. It should be noted that the three splitter plates have different lengths equal to $20h$, $15h$, and $10h$ for the TTE, ITE, and BTE cases, respectively. However, the upstream part of each plate (of constant thickness h) has the same length equal to $10h$ for the three geometries. The three configurations are presented in Fig. 1. The Reynolds number Re_{ML} based on the velocity difference $U_1 - U_2$ (where U_1 is the high-speed velocity and U_2 the low-speed one) and h is $Re_{ML} = 400$. The Reynolds number Re_W based on the mean convection velocity $U_c = (U_1 + U_2)/2$ and h is $Re_W = 1000$. The Reynolds numbers considered here by DNS are significantly lower than the one associated with the experiments in Ref. 14 for the TTE and BTE cases, where Re_{ML} was equal to 14 400 and Re_W to 36 000. Note finally that the velocity ratio $r = U_2/U_1 = 2/3$ and the modified velocity ratio $\lambda = (U_1 - U_2)/(U_1 + U_2) = 0.2$ remain the same for the three cases.

The boundary layers of thicknesses (corresponding to δ_{99}) $\delta_1 = 0.57$ and $\delta_2 = 0.5$ are laminar with a Blasius profile imposed at the inlet. They are submitted to residual 3D perturbations allowing a realistic destabilization of the flow downstream the trailing edge. The spectral content of this artificial perturbation is imposed to avoid the excitation of high wave numbers or frequency waves that cannot be correctly described by the computational mesh. It is important to stress that the Reynolds numbers $Re_{\delta_1} = 684$ and $Re_{\delta_2} = 400$ based on the free stream velocity and the boundary layer thicknesses are too small to expect any turbulent development of the boundary layers with this artificial generation of noise.

Even if the length of the trailing edge is not the same for each case, we use exactly the same inflow conditions for the
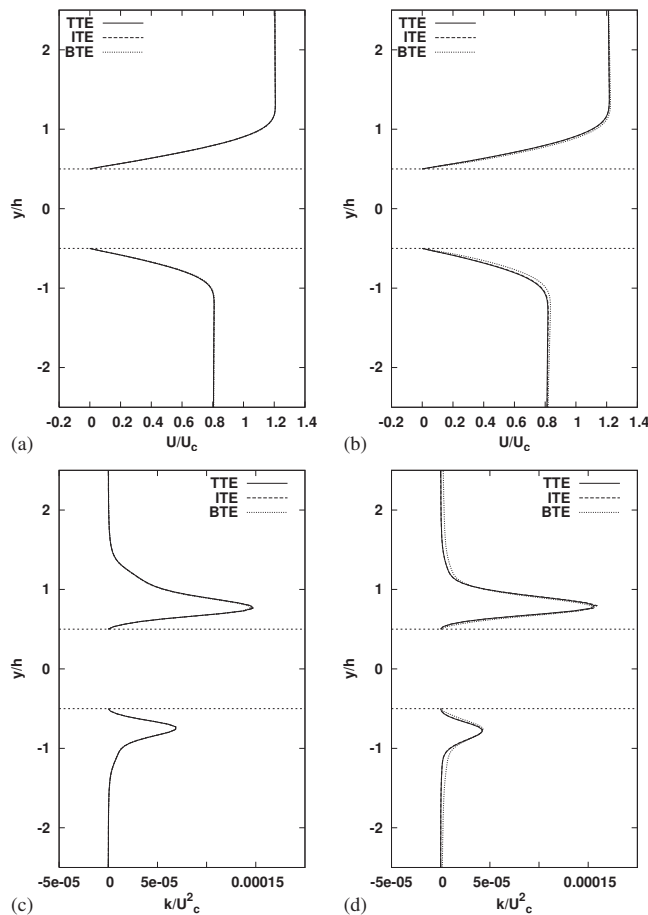
FIG. 2. Comparisons of the mean velocity profile [(a) and (b)] and the fluctuating kinematic energy profile [(c) and (d)] for the boundary layers, $4h$ [(a) and (c)] and $8h$ [(b) and (d)], downstream of the inlet section for the three geometries.

three geometries. The boundary layer evolutions are presented in Fig. 2 through comparisons of the mean velocity profile and fluctuating kinematic energy, $4h$ and $8h$, downstream of the inlet section. It should be noticed that the fluctuating kinematic energy injected at the inflow is relatively small with a maximum value of $\approx 0.000\,15 U_c^2$, $4h$ downstream of the inlet section, confirming that present boundary layers can be seen as mainly laminar.

It should be noted that in a previous numerical work,[22] we have considered simulations for the TTE and BTE cases without any inflow perturbations. Even if the mixing layers were not stable, the resulting dynamics was found unrealistic for the TTE case with no 3D motion inside the computational domain and with results virtually identical to those obtained for the corresponding two-dimensional (2D) DNS. It was due to the lack of 3D excitations required to trigger 3D instabilities.

Finally, a preliminary study has established that the collection time needed in the simulations to obtain correct and well converged low-order moment statistics in the mixing-layer region after the trailing edge is $T = 300h/U_c$, obtained after a transient stage to get a well established flow. Statistics are obtained by averaging over this time with an additional average in the periodic and statistically homogeneous

z-direction. Furthermore, in a preliminary study, we also have investigated the effect of the Reynolds number by performing a DNS of the turbulent flow generated by the BTE with a Reynolds number 50% higher ($\mathrm{Re}_{ML} = 600$) than the one used in this study. This simulation, using approximately 2.5 times more mesh nodes than the BTE case presented in this paper, did not show any significant differences in the streamwise evolution of the flow dynamic as far as present conclusions of this work are concerned. For this reason, only the moderate Reynolds number ($\mathrm{Re}_{ML} = 400$) is presented here.

B. Numerical methods

To solve the incompressible Navier–Stokes equations, we use an in-house code (called "INCOMPACT3D") based on sixth-order compact schemes for spatial discretization and second order Adams–Bashforth scheme for time advancement. To treat the incompressibility condition, a projection method is used, requiring to solve a Poisson equation for the pressure. This equation is fully solved in the spectral space via the use of relevant 3D fast Fourier transform that allows us to consider all the combinations of free-slip, periodic, or Dirichlet boundary conditions on the velocity field in the three spatial directions. In present calculations, boundary conditions are only inflow/outflow in x (velocity boundary conditions of Dirichlet type), free slip in y for $-L_y/2$ and $L_y/2$, and periodic in z for $-L_z/2$ and $L_z/2$. Note that in this paper, the origin in the streamwise direction is located at the end of each trailing edge in order to make easier comparisons. The pressure mesh is staggered from the velocity mesh to avoid spurious pressure oscillations. Using the concept of modified wavenumber, the divergence free condition is ensured up to the machine accuracy. More details about the present code and its validation, especially the original treatment of the pressure in spectral space, can be found in Ref. 23.

In order to take into account the wake effect introduced by the trailing edge, the geometry of the splitter plate is explicitly resolved, with an IBM, following the procedure proposed in Refs. 21 and 24. The present IBM is a direct forcing approach that ensures the no-slip boundary condition at the wall while creating an artificial flow inside the body. This internal flow, without physical significance, allows better regularity of the velocity field across the immersed boundary, this property being of primary importance when numerical schemes of spectral or quasispectral accuracy are used. Combined with a sixth-order compact filtering of the convective terms, this specific IBM leads to a reduction in wiggles in the neighborhood of the trailing-edge while allowing better quantitative predictions at marginal resolution (see Refs. 21 and 24 for more details).

For the TTE and BTE cases, the computational domain $(L_x \times L_y \times L_z) = (108h \times 96h \times 13.5h)$ is discretized on a Cartesian grid (stretched in y) of $(n_x \times n_y \times n_z) = (961 \times 257 \times 120)$ mesh nodes. For the ITE case, because of the unusual streamwise development of the flow dynamic, the computational domain is 50% longer in the streamwise direction with $L_x = 162h$ discretized with $n_x = 1441$. The stretching of the

grid in the y-direction leads to a minimal mesh size of $\Delta y_{min} \approx 0.03h$. The time step $\Delta t = 0.005h/U_c$ is low enough to have a Courant–Friedrich–Levy condition of about 0.3.

C. POD analysis

POD offers particular advantages pertinent to the present study. The objective of including POD is to try to identify the relevance and contribution of different modes to the behavior observed for each flow configuration. More information about POD can be found in Ref. 25. Different types of POD approaches can be used. Experimentally, this decision is dictated by the measurement technique, i.e., for time-accurate measurements for which the spatial resolution is poor, such as hot wire, classical POD can be used.[26] For measurement techniques with good spatial accuracy but poor temporal resolution, such as particle image velocimetry (PIV),[27] the use of snapshot POD was suggested. The analysis of experimental results for a plane mixing layer, at a Reynolds number equivalent to the one use in present work, was presented in Ref. 28. They showed that in the early stage of the mixing, most of the fluctuating energy is carried by very few modes and that the first two pairs of mode represents convective instabilities, with a phase angle of $\pi/8$ between two modes of each pair. However, their analysis was 2D and limited to the region where Kelvin–Helmholtz vortices are still mainly homogeneous in the spanwise direction (no helicoidal modes). We propose to go further and analyze the full 3D dynamics for each simulation.

The *snapshot* variant has been applied herein, using 480 3D snapshots, regularly sampled over 240 time units. The velocity field is decomposed into a sum of modes, each multiplied with a corresponding time-dependent coefficient,

$$u_i(x,y,z,t) = \sum_{n=1}^{N} a^n(t)\Phi_i^n(x,y,z), \tag{1}$$

where $u_i(x,y,z,t)$ denotes the velocity component i, $a^n(t)$ are the time-dependent (so-called random) coefficients and are representative of the flow dynamic, and the eigenfunctions $\Phi_i^n(x,y,z)$ are representative of the flow organization. Since the flow is statistically homogeneous in the spanwise direction, the empirical eigenfunctions can be regarded as plane waves[29] and take the form

$$\Phi_i^n(x,y,z) = \xi_i^q(x,y,k)\exp(-\iota kz) \tag{2}$$

with

$$k = 2\pi m/L_z, \tag{3}$$

where q is the so-called quantum number and m is the number of full waves in the homogeneous z-direction.

III. NEAR TRAILING-EDGE REGION

A. Instantaneous flow visualizations

Figure 3 shows top and side views of enstrophy isosurfaces for the three different simulations, for the first half of the computational domain in the streamwise direction for $-10h < x < 44h$. For the BTE and TTE, a fully 3D dynamic can already be observed close to the trailing edge, with the

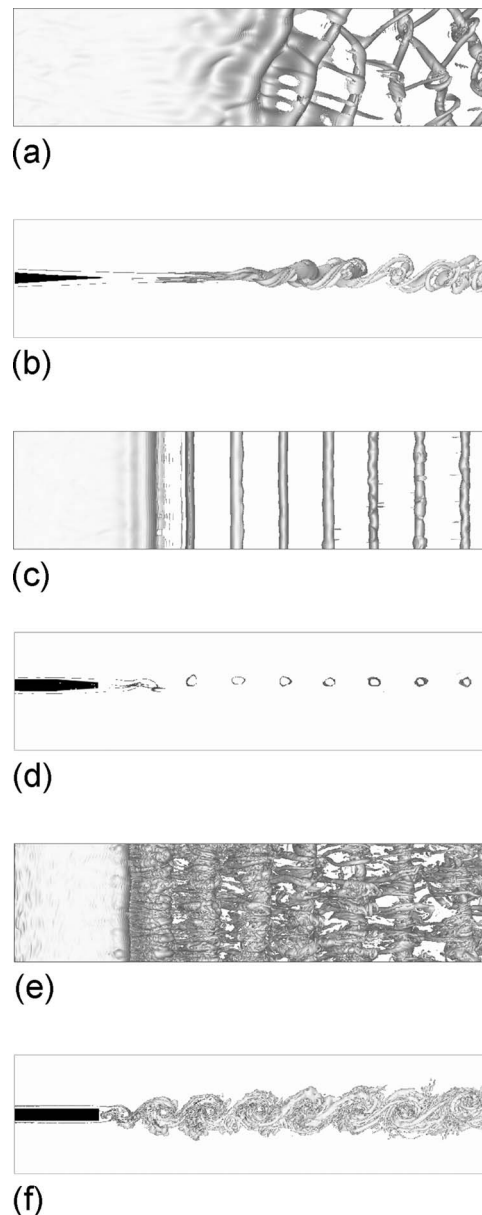
(a)

(b)

(c)

(d)

(e)

(f)

FIG. 3. Side and top views of enstrophy isosurface for the cases with a thin splitter plate [simulation TTE, (a) and (b)], an intermediate trailing edge [simulation ITE, (c) and (d)], and a blunt trailing edge [simulation BTE, [(e) and (f)] for $-10h < x < 44h$.

presence of large-scale spanwise structures, but with a different flow dynamics between the two configurations.

The early instabilities lead to the creation of large spanwise vortices for the TTE case, which are then submitted to 3D helicoidal pairing, characteristic phenomenon of a mixing layer disturbed by a 3D perturbation. This observation is in good agreement with previous experimental[9,30] and numerical observations[10,31] (see Ref. 4 for an extended review on this topic).

Enstrophy visualizations obtained in the BTE case suggest clearly that the mechanisms associated with the self-excitation of the flow allow a highly 3D turbulent state immediately behind the trailing edge. This drives the layer to an asymmetric vortex shedding where vortices of negative spanwise vorticity [of the same sign as the shear given by $-(U_1$
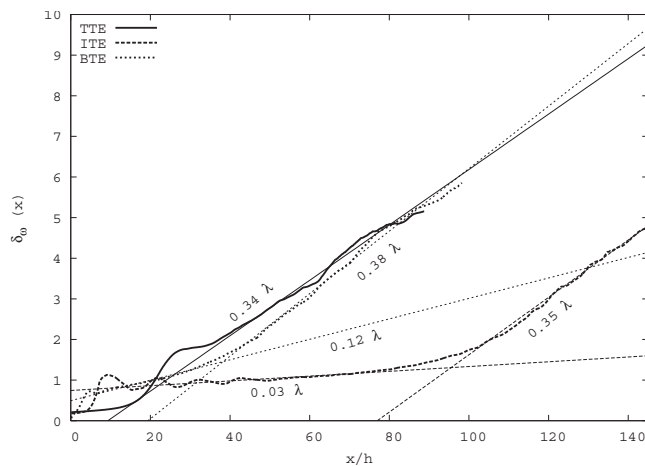
FIG. 4. Streamwise evolution of the vorticity thickness. The origin of each case is located at the trailing edge of the splitter plate.

$-U_2)/h]$ are promoted while their positive counterparts vanish as the flow evolves in the streamwise direction. It should be noted that no pairing can be observed in the first part of the flow, which seems to indicate that the wake effect is playing a key role in the flow dynamics by delaying the pairing (by comparison with the TTE case where some helicoidal pairing can be observed close to the trailing edge).

For the ITE case, only a 2D dynamic can be observed in the first half of the computational domain, with a lack of strong longitudinal vortices between the large-scale spanwise structures. Even if the boundary layers have been disturbed by 3D perturbations, it seems that the shape of the splitter plate clearly favors the development of 2D primary structures. Moreover, these large-scale vortices, oriented in the spanwise direction with a negative vorticity as in the TTE case, are found to be clearly more stable with respect to 3D perturbations compared to the two other cases.

A careful examination of the vortex shedding process in the ITE case reveals that the formation of the primary structure leads to vortices that are elongated in the horizontal direction when they detach from the trailing edge. Then, each detached vortex keeps its shape while rotating around its center while it is convected further downstream. This specific vortex shedding leads to a phase locking for the rotation of the elongated structures hence formed for a given x-location, explaining the wavy behavior of the vorticity thickness that can be observed for the ITE case in Sec. III B in Fig. 4. Note that we have checked in a preliminary 2D DNS of the same case that the wavy evolution of the vorticity thickness cannot be attributed to the lack of convergence, this wavy behavior being also recovered for a very long time of integration.

B. Statistics

Figure 4 shows the streamwise evolution of the vorticity thickness for each simulation. For the TTE case, after an initial moderate laminar growth just downstream of the trailing edge, the vorticity thickness grows quickly and then follows a linear evolution from $x \approx 35h$, with a spreading rate of $d\delta_\omega/dx \approx 0.34\lambda$, slightly overestimated with previous com-

putational results in Ref. 10 which reported a maximum growth rate of 0.27λ. As already mentioned in Ref. 9, there is a wake effect behind the trailing edge (even a thin one), especially when the ratio U_2/U_1 is relatively important. Indeed, in this experimental study, the mixing layer did not achieve self-similarity within the measurement domain because of this wake effect. Such an effect, which cannot be taken into account in a simulation where the flow is generated with a hyperbolic profile, could be responsible here for the overestimated growth rate of the vorticity thickness.

The evolution of the vorticity thickness for the BTE case can be divided into three parts: a rapid growth, up to $x=4h$, followed by a slow spreading ($d\delta_\omega/dx \approx 0.12\lambda$, from $x=4h$ to $x=45h$) and then a much higher spreading rate ($d\delta_\omega/dx \approx 0.38\lambda$). The lowest spreading rate in BTE case (with respect to TTE case) in the second part of the evolution can be interpreted as a logical consequence of the delay observed in the instantaneous visualizations for the pairing close to the trailing edge. Further downstream, the sudden increase in the spreading rate (from $x=45h$) leads virtually (inside the uncertainty range for the present statistical convergence) to a bigger value by comparison with the TTE case (0.34λ for the TTE case against 0.38λ for the BTE case). This behavior will be discussed in Sec. IV where the far trailing-edge region is studied. The evolution of the vorticity thickness for the BTE case is qualitatively consistent with the experimental results in Ref. 12 where a significant increase in the vorticity thickness was observed compared to the TTE case. Note also that in Ref. 13, the slow and rapid growths of the vorticity thickness for the BTE case were also exhibited but with a level of statistical convergence that was three times smaller than in the present work.

The vorticity thickness for the ITE case can also be divided into three parts: an oscillating region up to $x=40h$, followed by a region with a very slow growth rate ($d\delta_\omega/dx \approx 0.03\lambda$) from $x=40h$ to $x=80h$, and then a more conventional growth rate ($d\delta_\omega/dx \approx 0.35\lambda$), which will be discussed in Sec. IV. As already mentioned, the wavy behavior observed close to the trailing edge for the vorticity thickness is a consequence of the elongated shape of the vortices formed behind the ITE. In agreement with the instantaneous visualizations, it seems that spanwise elongated vortices are generated just behind the trailing edge, are convected downstream, and are rotating on themselves leading to these unusual oscillations on the vorticity thickness. As already mentioned previously, this wavy behavior is a consequence of the phase locking mechanism in the rotation of the elongated shedded vortices that can be clearly exhibited on a full 3D animation of the enstrophy using more than 300 fields (not presented here).

The mean flow patterns obtained for each simulation are presented in Fig. 5 where some selected streamlines are plotted to highlight the length and shape of the recirculation region observed just downstream the trailing edge. As expected, it is not possible to observe a recirculation region for the TTE case. Indeed, the added bevel has been carefully chosen to avoid any flow separation, with a very smooth slope. For the BTE and ITE cases, we can observe an asymmetric pattern of the mean streamlines due to the velocity
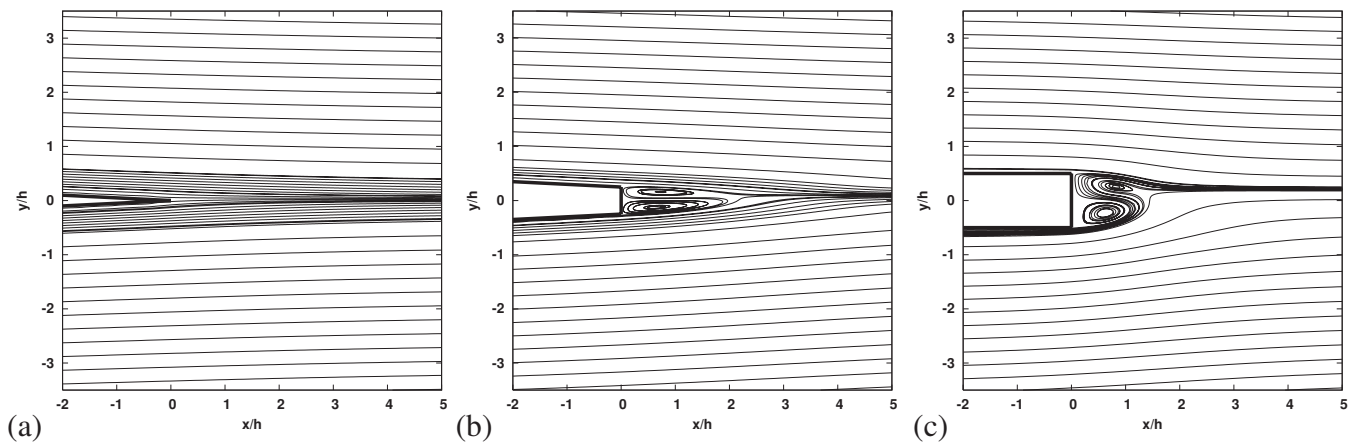
FIG. 5. Velocity streamlines for each simulation, just downstream of the trailing edge. The origin of each case is located at the trailing edge of the splitter plate: (a) TTE, (b) ITE, and (c) BTE.

difference $U_1 - U_2$, with a recirculation region downstream the splitter plate because of the thickness of the trailing edge, introducing a strong wake effect. It should be noted that for the ITE case, this recirculating region is more elongated than for the BTE case, leading to the slightly elongated shape of the large-scale spanwise structures observed in the instantaneous visualizations of enstrophy. This unusually large (in the streamwise direction) recirculation region could be partly responsible of the lack of 3D motions observed in the region close to the trailing edge. Finally, it should be noted that the shape of the recirculation region for the BTE case leads to more conventional rounded large-scale spanwise structures downstream of the trailing edge.

As shown in Fig. 6 on the mean streamwise velocity, the wake influence diminishes very quickly for the TTE case. It should be noticed that the transverse velocity fluctuations are higher than in previous numerical work[10,31] and are bigger than the streamwise ones. This overestimation can be interpreted as the signature of a more marked 2D dynamics compared to previous numerical studies where the wake component was not taken into account. Note finally that the maximum fluctuations are observed on the high velocity side, which is not in agreement (for the TTE case) with the experiments in Ref. 14 and with previous spatial simulations in Ref. 10. For the BTE case, the wake component remains significant in the near trailing-edge region. For the streamwise velocity fluctuations, we can observe two extrema: one on the high velocity side and one on the flow axis ($y/h=0$), corresponding to the recirculation region. Further downstream, this quantity has only one minimum on the high velocity side. Note also that the streamwise and spanwise velocity fluctuations are much higher, close to the trailing edge with respect to the TTE case. The maximum fluctuations are located on the high velocity side in agreement (for the BTE case) with the experiments in Refs. 12 and 14. For the ITE case, the wake component is also found significant for the computational domain considered here. We can observe three extrema for the streamwise fluctuations: a big one on the high velocity side, a small one on the low velocity side, and one in the axis of the flow for $y/h=0$. The latest one is related to the elongated recirculation bubble already ob-

served downstream of the trailing edge. Note that this extremum on the axis of the flow exists also for the BTE case. The transverse velocity fluctuations for the BTE and ITE cases are much higher than in the TTE case, which is the signature of a flow mainly driven by 2D motions. As expected, the spanwise velocity fluctuations for the ITE case remain very close to zero as no 3D motion can be observed for this configuration.

In order to interpret the different behaviors of each flow and to better understand the flow dynamic for each simulation, let us consider the linear stability properties expected of each mixing layer. Following the idea introduced in Ref. 15, the problem can be considered in terms of convective and/or absolute instability. Indeed, the authors in Ref. 15 showed that for a hybrid wake-/mixing-layer profile,

$$U(y)/U_c = 1 - f \, \text{sech}^2(y/\delta) + \lambda \, \tanh(y/\delta), \qquad (4)$$

the corresponding flow becomes absolutely unstable for $f > 0.95$, where f is the wake deficit parameter (i.e., the velocity deficit divided by the mean convection velocity) and λ corresponds to the modified velocity ratio of the mixing layer. The authors in Ref. 13 showed that this generic profile is a good approximation of the mean streamwise velocity profile U and therefore f can be obtained through the relation

$$f(x) = (U_c - \min_y U)/U_c. \qquad (5)$$

It should be noted that an absolutely unstable region must be expected for each mixing layer due to the boundary condition on the trailing edge that implies $f(0)=1$.

Figure 7 shows the streamwise evolution of the wake deficit parameter f for each simulation. The area where $f > 0.95$ is clearly more important for the ITE where the flow is absolutely unstable for $0 < x/h < 2.7$ whereas it is absolutely unstable for $0 < x/h < 0.27$ and $0 < x/h < 1.35$ for the TTE and BTE cases, respectively. Based on these observations, it is reasonable to think that the ITE case leads to a flow globally unstable (self-excited flow with vortex shedding, with a relatively poor receptivity to inflow perturbations) while the TTE case leads to a flow with a strong sensitivity to inflow perturbations with characteristics of a
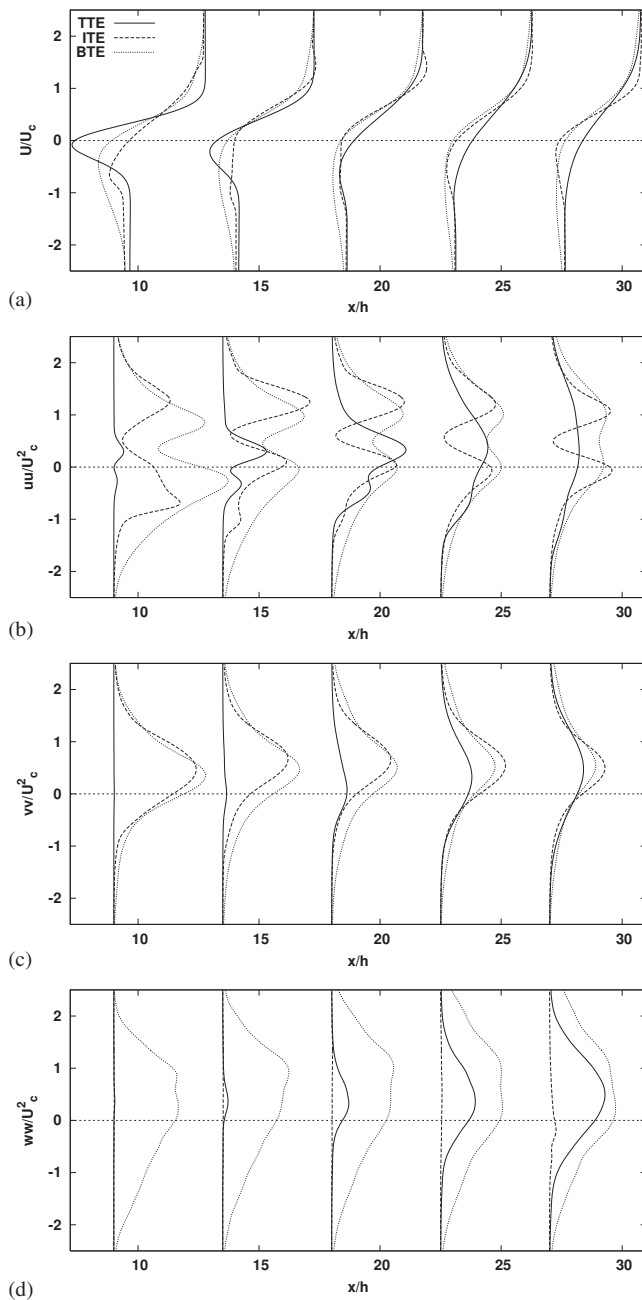
FIG. 6. Profiles of: (a) the mean streamwise velocity (increased by a factor 8), (b) the streamwise velocity fluctuations (increased by a factor 150), (c) the transverse velocity fluctuations (increased by a factor 50), and (d) the spanwise velocity fluctuations (increased by a factor 300) for each simulation at five different streamwise positions in the near trailing-edge region (every $4.5h$ from $9h$).
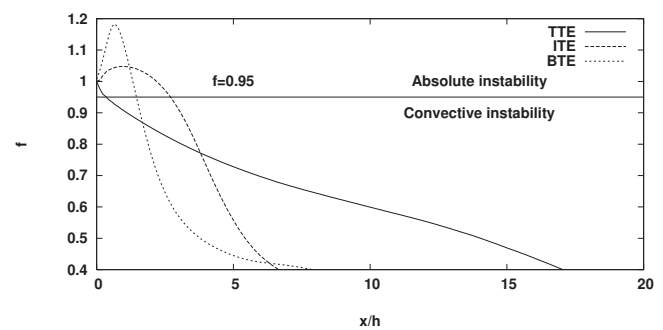

FIG. 7. Streamwise evolution of the wake deficit parameter [Eq. (5)] in the near trailing-edge region for each simulation.

nal flow field onto the first four eigenmodes gives the time evolution of the coefficients $a^n(t)$ shown in Fig. 9. Modes can be grouped in pairs because the energy associated with each odd mode is very similar to that associated with the following even one, with the time evolution shifted by $\pi/4$ within any one pair (see Fig. 9), and there is also a corresponding shift in space in the mode shapes. Hence, only the odd modes are shown in Fig. 8.

For the TTE case [Fig. 8(a)], modes 1 and 2 are very similar to that observed experimentally in Ref. 28, which used PIV measurements. Those modes are associated with the subharmonic instability wave. The first two modes are translated from one to another by a quarter wavelength, confirming the convective nature of those modes. It was shown in Ref. 28 that the modes reach their maximum energy when they are vertically aligned. It occurs, for the TTE case, at the end of the domain shown in Fig. 8(a), corresponding to the location where the vorticity thickness changes from a quasi-laminar (i.e., dominated by very few modes) to a more turbulent one. An interesting behavior is the fact that modes (3,4) and (5,6) have the same spanwise wavenumber with the same frequency as mode (1,2). Those modes are associated with one spanwise oscillation ($m=1$) and correspond to helicoidal instabilities, a phenomenon not described in the experiments in Ref. 28 because of measurement limitations. Indeed, time history [Fig. 9(a)] shows that when mode pair (1,2) are the most energetic [$a^1(t)$ reaches its maximum amplitude], the energy carried by the other modes decreases [$a^n(t) \approx 0$ for $n=3$ and 4], and conversely, when both (3,4) and (5,6) show strong amplitude, the amplitude of $a^1(t)$ and $a^2(t)$ is reduced. From a dynamical perspective, it shows that a 3D instability is dominating the flow. Structures associated with the fundamental instability waves are carried by higher and less energetic modes (not shown here for compactness).

The transverse component of the eigenvectors [Fig. 8(c)] and the associated temporal coefficient [Fig. 9(c)] for the BTE case are very different from those of the TTE case. The structures of transverse component ξ_2^q are almost always vertical, as it is usually observed in wake flows, where structures are purely convected. A slight variation of shape is observed on the lower (low velocity side) side of the mode shapes, but this does not seem to affect significantly the flow dynamic. Higher modes [e.g., mode pair (3,4)] show the typical instability waves of wake flows, and the initial disturbances associated with the asymmetric (top-bottom) wake

convectively unstable flow. The flow generated in the BTE case can be seen as an intermediate flow between these two cases but with a large enough absolutely unstable area to expect a globally unstable behavior as for the ITE case.

C. POD

The shape of the transversal component of the eigenvector ξ_2^q, corresponding to the first four modes, is shown in Fig. 8, and the associated energy, for each mode, is given in Table I. The projection of the velocity fluctuations from the origi-
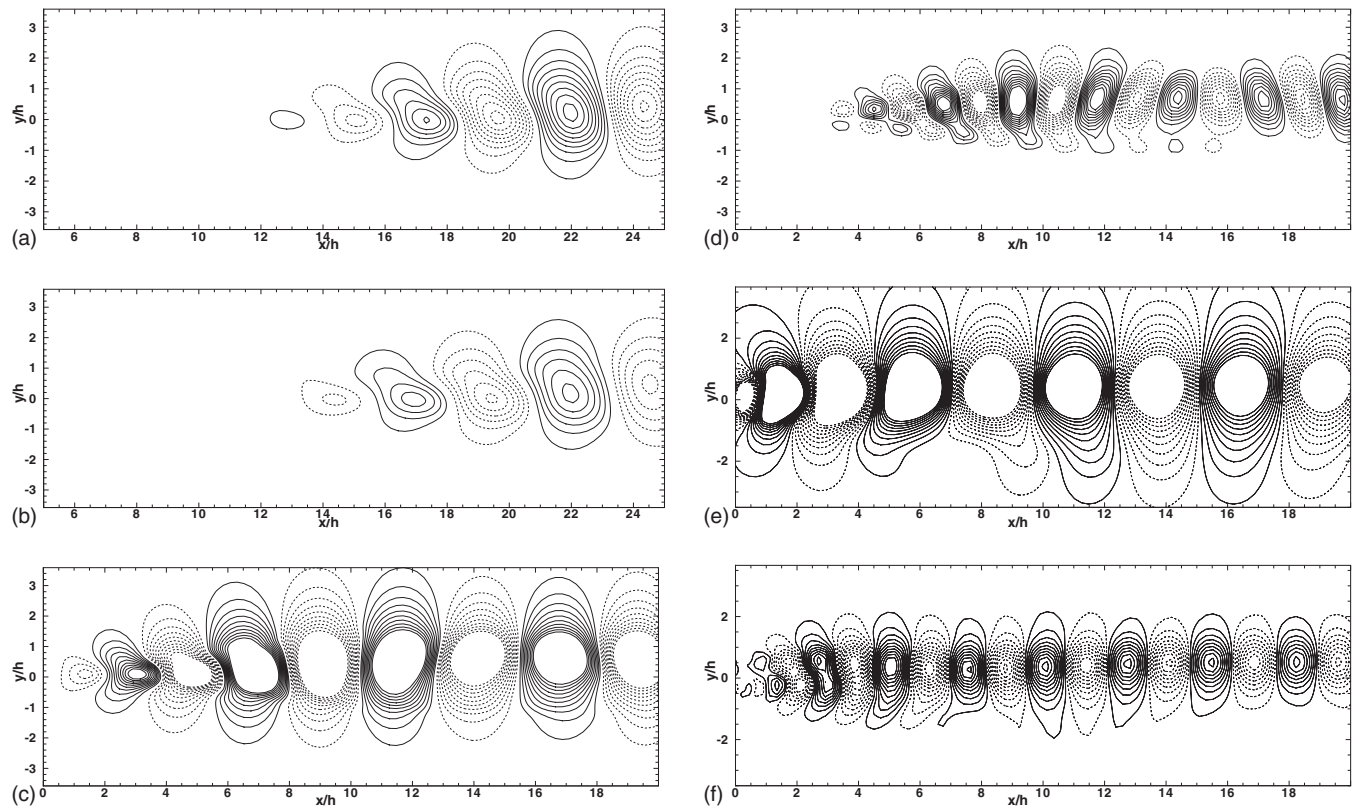
FIG. 8. Isocontours of the transverse POD component for each case: [(a) and (d)] TTE, [(b) and (e)] ITE, and [(c) and (f)] BTE, for $n=1$ (left) and $n=3$ (right).

flows (observed between $x/h=0$ and $x/h=4$) are disappearing quickly. In that case, the asymmetric wake component does not seem to affect the overall flow behavior. The temporal coefficients [Fig. 9(c)] are purely harmonic, with a frequency typical of wake flows.

The mode shape for the ITE case [Fig. 8(b)] differs from the two other cases. On one hand, mode pair (1,2) is similar to mode (1,2) of BTE [Fig. 8(c)], with identical streamwise wavelength, and same vertical alignment of structures. Mode (3,4), on the other hand, differs greatly from that of the BTE case, and resembles more that of the TTE case (with different streamwise wavelength). Indeed, the structures are tilted as the flow evolves downstream (energy transfer from the mean flow to the fluctuations, with a maximum of energy when the structures are vertically aligned, around $x=9h$). From $x=12h$, the flow structures are tilted at an acute angle with the positive streamwise direction, involving a loss of energy to

the mean flow, and then split into two smaller structures, with the same frequency but with a different wavelength. This phenomenon has been called *mode degeneration* in Ref. 28. It is assumed to enhance entrainment and mixing. The

TABLE I. Relative energy (in %) carried by each mode. The spanwise wavenumber of each mode is also given between parentheses.

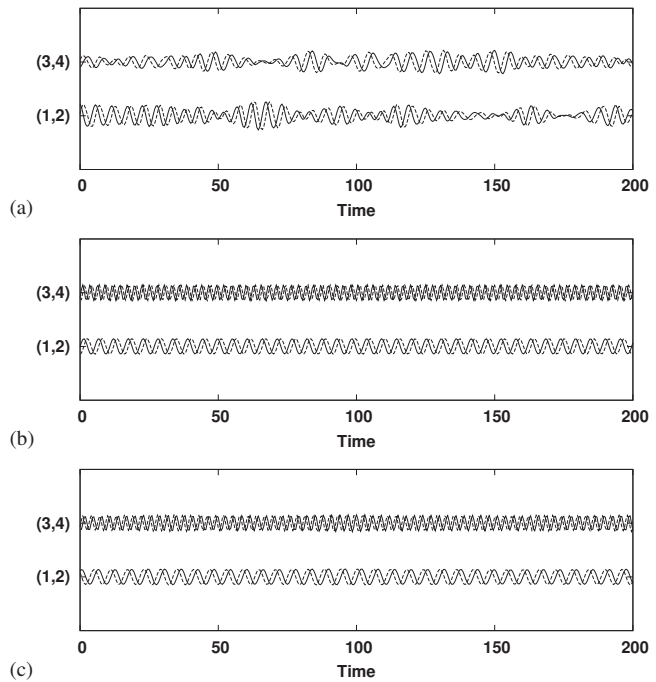| Mode n	TTE	ITE	BTE
1	11.7 $(m=0)$	41.0 $(m=0)$	34.7 $(m=0)$
2	11.1 $(m=0)$	40.1 $(m=0)$	34.1 $(m=0)$
3	7.5 $(m=1)$	7.0 $(m=0)$	3.8 $(m=0)$
4	7.4 $(m=1)$	6.9 $(m=0)$	3.7 $(m=0)$
5	4.8 $(m=1)$	1.3 $(m=0)$	0.6 $(m=0)$
6	4.8 $(m=1)$	1.2 $(m=0)$	0.6 $(m=0)$

FIG. 9. Time evolution of the random coefficients $a^n(t)$ for each case: (a) TTE, (b) ITE, and (c) BTE.
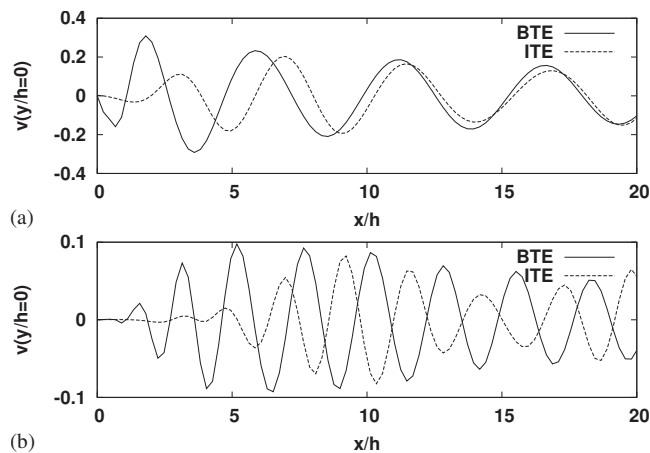
(a)

FIG. 10. Streamwise evolution of the vertical component of the (a) first and (b) third POD modes, for the BTE and ITE cases, on the center line of the flow for $y/h=0$.
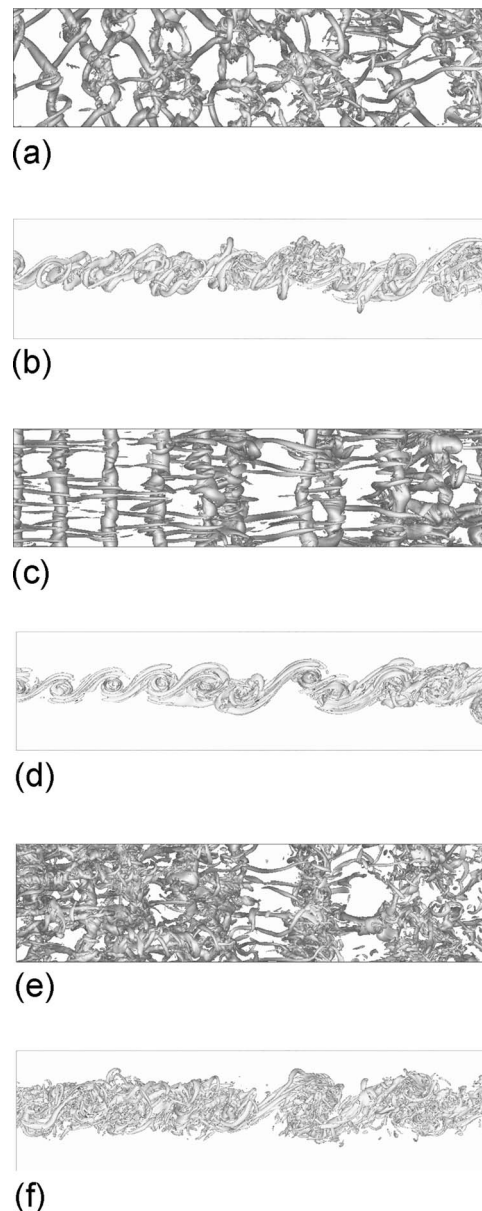

FIG. 11. Side and top views of enstrophy isosurface for the cases with a thin splitter plate [simulation TTE, (a) and (b)], an intermediate trailing edge [simulation ITE, (c) and (d)], and a blunt trailing edge [simulation BTE, (e) and (f)] for $54h<x<108h$ for the TTE and BTE cases and for $108h<x<162h$ for the ITE case.

mode shape for the ITE case hence shows that two different behaviors are competing: the dominating modes are associated with the wake effect, while the secondary modes (3,4) are mixing-layer type. In any case, the modes are spanwise homogeneous ($m=0$ for the first six modes, representing about 98% of the total fluctuating energy), and the temporal coefficients again display a purely harmonic behavior.

A direct comparison of the structure wavelength between BTE and ITE cases is shown in Fig. 10, by comparing the vertical component of the first and third POD modes on the flow axis ($y/h=0$). Instabilities occur on the center line in the shear layer downstream from the recirculating region where the center line streamwise velocity becomes positive. Hence, because the recirculation bubble is longer for ITE case than for BTE case, instabilities "kick in" earlier in the latter case. However, the maximum amplitude is reached at $x/h=2$ (while recirculation bubble is $\approx 1.5h$ long) for modes 1 and 2 (the most energetic ones), and then the amplitude decreases, while for the ITE case, the maximum is reached further downstream (at $x/h\approx 7$, with a bubble finishing at $x/h\approx 2.5h$). Finally, despite its asymmetric character, the occurrence of an alternate vortex shedding in the BTE case leads to a vortex street that seems to be more stable with respect to subharmonic perturbations compared to the Kelvin–Helmholtz rollers formed in the TTE case.

Due to present differences in vortex dynamics, it seems logical to expect important changes in the flow dynamics for each configuration in the far trailing-edge region of the flow. This point will be addressed in Sec. IV.

IV. FAR TRAILING-EDGE REGION

A. Instantaneous flow visualizations

The behavior in the far trailing-edge region is assumed, in many papers, to be more universal and most of the time, a self-similar state can be reached relatively close to the trailing edge. However, some experiments[9] and simulations[7,13] have shown that the wake effect (introduced by a thin or a thick trailing edge) could be significant even far downstream from the splitter plate, even if it is difficult to quantify it

locally. Reference [9], in particular, showed that the wake effect increases with the increase in the ratio U_2/U_1, but this study was based on a flow generated by a thin splitter plate.

Instantaneous visualizations of the enstrophy at the end of the computational domain for each simulation are presented in Fig. 11. For the TTE case, it can be observed that 3D motions are in qualitative agreement with reference studies on the spatially developing mixing layer (see, for instance, Ref. [10]), where the typical flow topology involving longitudinal structures stretched between large spanwise rolls and helicoidal pairing is well recovered here. A gradual disappearance of the large spanwise structures can be visually detected at the end of the computational domain. For the BTE case, at least one pairing can be clearly observed which
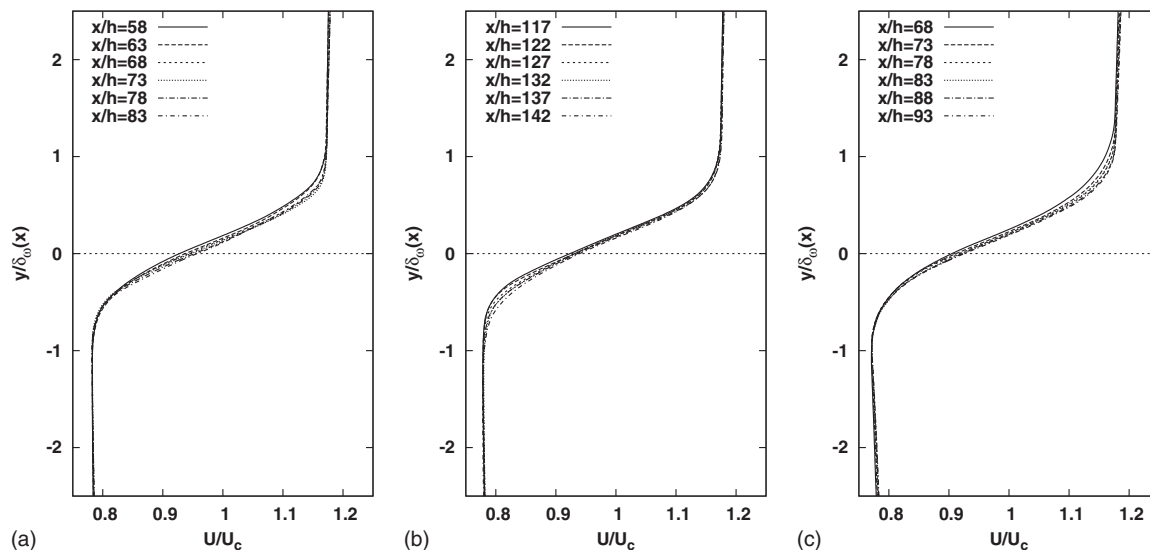
FIG. 12. Streamwise velocity profiles for each simulation at six different streamwise locations in the far trailing-edge region, every $5h$: (a) TTE, (b) ITE, and (c) BTE.

seems to show that the wake effect disappear with a more limited effect on the flow dynamic in the far trailing-edge region. It is well known that pairing contributes strongly to the expansion of a mixing layer. Therefore, we could expect to have the same streamwise evolution for the vorticity thickness (discussed in Sec. IV B) for the TTE and BTE cases. Again, the large-scale spanwise coherence of structures starts to vanish at the end of the computational domain through their twist by small-scale streamwise vortices. One of the main important points for the ITE case is that the flow dynamic finally becomes 3D with the occurrence of streamwise vortices stretched between the large-scale spanwise structures. However, these structures are still dominant for the ITE case, which confirms that the flow remains strongly influenced by the shape of the trailing edge. Unfortunately, the computational domain is not long enough to investigate further downstream the evolution of the flow and to see if the wake effect will finally disappear as it is observed for the others cases.

B. Statistics

The evolution of the vorticity thickness for the whole computational domain is shown in Fig. 4 for each simulation. As expected and because of the different flow dynamics observed for each case, each simulation leads to a different growth rate for the vorticity thickness. However, all the values obtained (0.34λ for the TTE case, 0.35λ for the ITE case, and 0.38λ for the BTE case) are overestimated by comparison to previous numerical and experimental investigations. Again, it is important to recall that this is one of the very first times, to our knowledge, that a mixing layer is not generated with a hyperbolic profile but with a thick splitter plate directly into the computational domain. Therefore, the wake effect, introduced by the trailing edge, combined with a

relatively small Reynolds number (by comparison with experiments) could be responsible for this overestimation.

Profiles for the mean flow velocity are presented in Fig. 12. The transverse direction is normalized by the local vorticity thickness. A self-similarity state can be observed for the TTE case and the profile does fit with classical hyperbolic tangent profiles (not presented here for clarity). For the BTE case, we can clearly see that the wake effect remains important locally even at the end of the computational domain. The ITE case can be seen here as an intermediate case, a self-similarity state being almost reached, and no wake effect can be clearly observed.

Some velocity fluctuation profiles for the three simulations are presented in Fig. 13. For these quantities, it is clear that no self-similar state is reached for all the three cases. The profiles for the BTE and TTE cases reach almost the same maxima for the streamwise and transverse velocity fluctuations with a gradual streamwise decrease in the maxima, located on the high velocity side. The fluctuation levels compare well with previous simulations.[10,31] The maximum observed in the region near the trailing edge and located on the axis of the flow has disappeared for the BTE case, which seems to confirm that the flow has almost forgotten the wake signature of the trailing edge, even if it is still visible on the mean streamwise profile in Fig. 12. It should be noted that for the TTE case, the spanwise velocity fluctuation profile remains almost the same in the far trailing-edge region while decaying for the BTE case.

The streamwise velocity fluctuation profiles for the ITE case are much sharper than the BTE and TTE ones while the transverse velocity fluctuation one is much larger than for BTE and TTE ones. It could be seen as a signature of a transitional mixing layer where the transverse/spanwise velocity fluctuations are over-/underpredicted, respectively, by
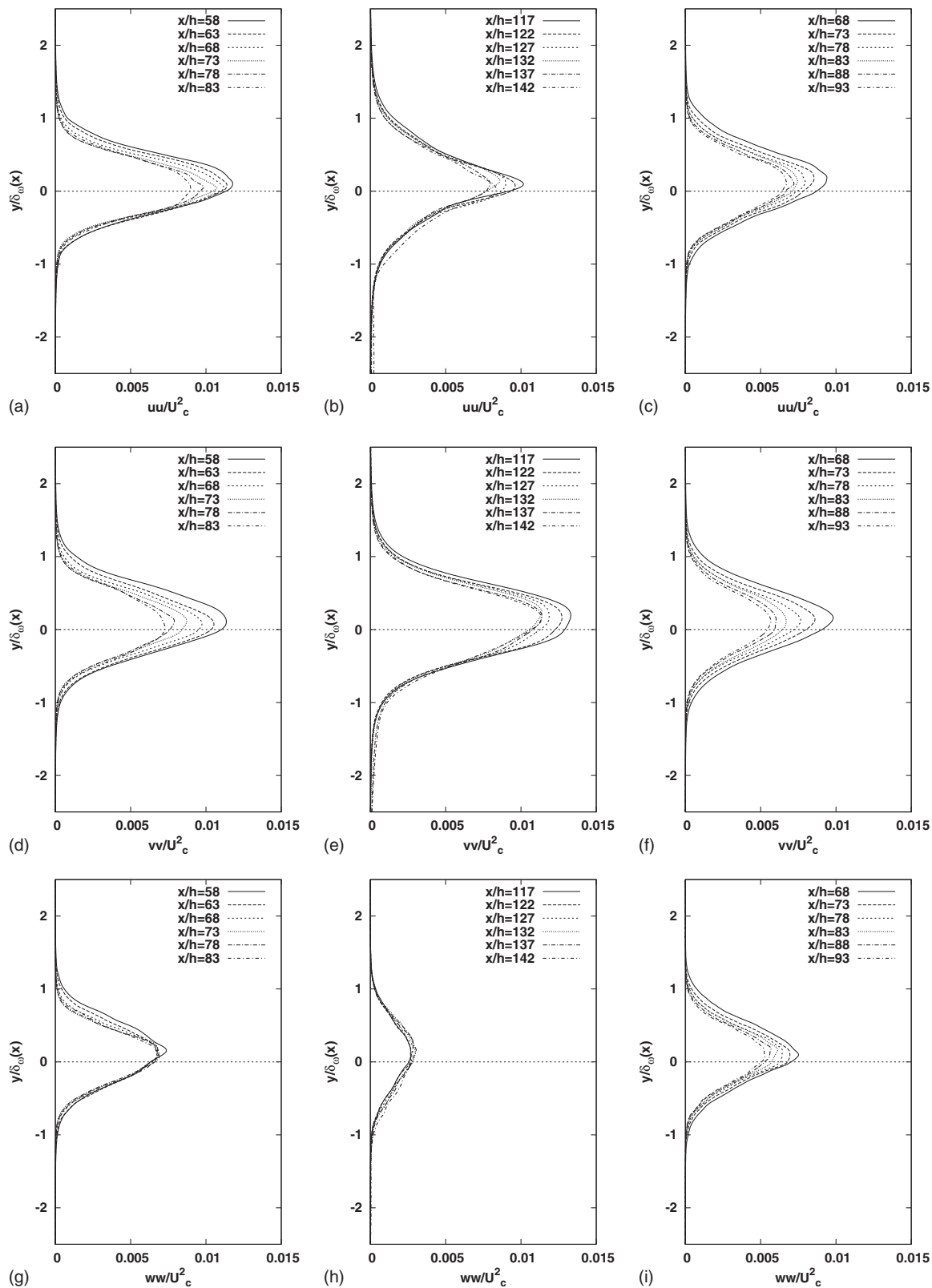
FIG. 13. Streamwise [(a)–(c)], transverse [(d)–(f)], and spanwise [(g)–(i)] velocity fluctuations for the three simulations at six different streamwise locations in the far trailing-edge region, every $5h$ for the TTE [(a), (d), and (g)], ITE [(b), (e), and (h)], and BTE [(c), (f), and (i)] cases.

comparison with self-similar turbulent mixing-layer results. Indeed, the maximum of the spanwise velocity fluctuation profile is about twice as small as in the ITE case, by comparison with the two other cases. This important result con-

firms that the flow is still governed by a 2D dynamic probably because of the elongated recirculation region generated by the truncated bevel, which is still affecting the flow even up to the far trailing-edge region.

TABLE II. Relative energy carried by each mode, for each case. The spanwise wavenumber of each mode is also given between parentheses.

Mode n	TTE	ITE	BTE
1	2.71 ($m=0$)	9.67 ($m=0$)	5.04 ($m=0$)
2	2.66 ($m=0$)	9.47 ($m=0$)	4.92 ($m=0$)
3	1.62 ($m=0$)	5.1 ($m=0$)	1.88 ($m=0$)
4	1.58 ($m=0$)	4.72 ($m=0$)	1.82 ($m=0$)
5	1.43 ($m=1$)	3.19 ($m=0$)	1.01 ($m=2$)
6	1.42 ($m=1$)	3.14 ($m=0$)	0.93 ($m=2$)
7	1.24 ($m=0$)	2.36 ($m=0$)	0.75 ($m=0$)
8	1.23 ($m=0$)	2.12 ($m=0$)	0.71 ($m=0$)

C. POD

As described in Sec. IV C, the flow dynamic further downstream of the trailing edge becomes almost turbulent with significant differences for the mean and fluctuating quantities. POD eigenvalues for all the three cases for the first four most energetic mode pairs are given in Table II. Associated transverse mode shapes are shown in Figs. 14–16, for the TTE, ITE, and BTE cases, respectively.

The time evolution of the coefficient $a^n(t)$ is shown in Fig. 17(a) for the first eight modes for the TTE case. The frequency associated with mode pair (1,2) is associated with the subharmonic frequency of the two most energetic modes, already observed in Sec. III C. By the end of the domain, the structures are tilted at a very acute angle to the streamwise direction (Fig. 14) i.e., losing energy to the mean flow.[28] The time evolution, shown for the full period, also exhibits a second modulation, which is the signature of pairings occur-

ring for each simulation at the end of the computational domain.[28] Structures in pairs (3,4) and (5,6) (Fig. 14) have similar streamwise wavelength and similar frequencies but have different spanwise wavenumbers (see Table II). The projection of the velocity snapshots on those modes shows a very low-frequency modulation of the random coefficients $a^n(t)$ [Fig. 17(a)], which are exactly out of phase: When large amplitudes are observed on $a^3(t)$ and $a^4(t)$, the amplitudes of $a^5(t)$ and $a^6(t)$ decrease and vice versa. Their energy peaks at approximately $x/h=70$.

Again, mode degeneration described above is observed on mode pair (7,8) (see Fig. 14). Interestingly, mode pair (5,6) shows a slightly longer streamwise wavelength than mode (1,2) (about 25% longer) with a lower frequency [see Fig. 17(a)]. Note also that mode pair (5,6) is not spanwise homogeneous, but all other modes are. This could mean that the domain is not wide enough to have a mode $m=1$ for the lower wavelength.

Very similar observations can be made for the BTE case: The flow is still dominated by the fundamental instability wave and its subharmonic [sinusoidal shape of the random coefficients, see Fig. 17(c)] with higher harmonics on mode pairs (3,4) and (7,8). Mode degeneration, described in Ref. 28 as the effect of modal interaction, is observed on mode pair (7,8). Another interesting phenomenon is the presence of elongated structures [mode (5,6)] with a spanwise wavenumber $m=2$ (i.e., higher wavenumber than expected). This may be attributed to the presence of energetic streamwise elongated structures, similar to those observed in Fig. 11.

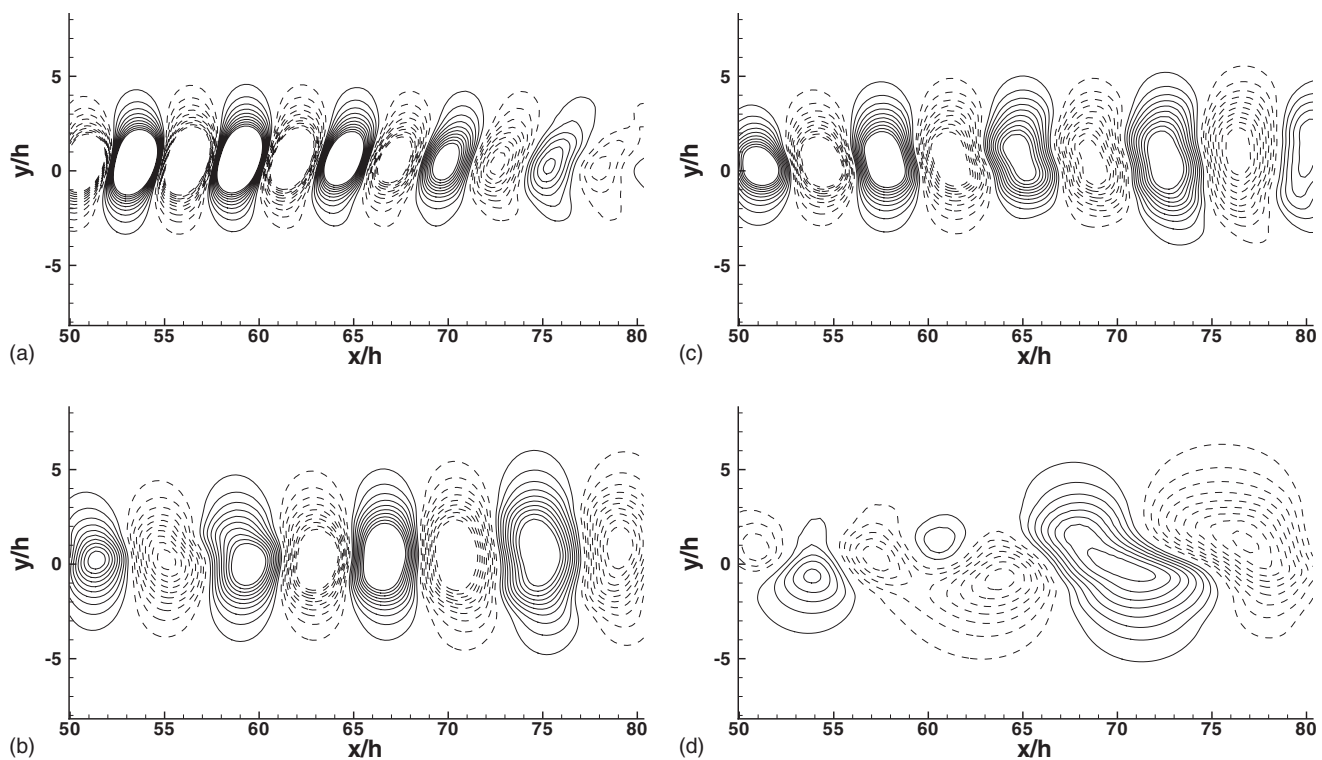For the ITE case [Figs. 15 and 17(b)], the flow remains mostly 2D ($m=0$ for the first eight most energetic modes)

FIG. 14. Isocontours of the transverse POD component ξ_2^q for the TTE case, for $q=1$ (a), 3 (c), 5 (b), and 7 (d).
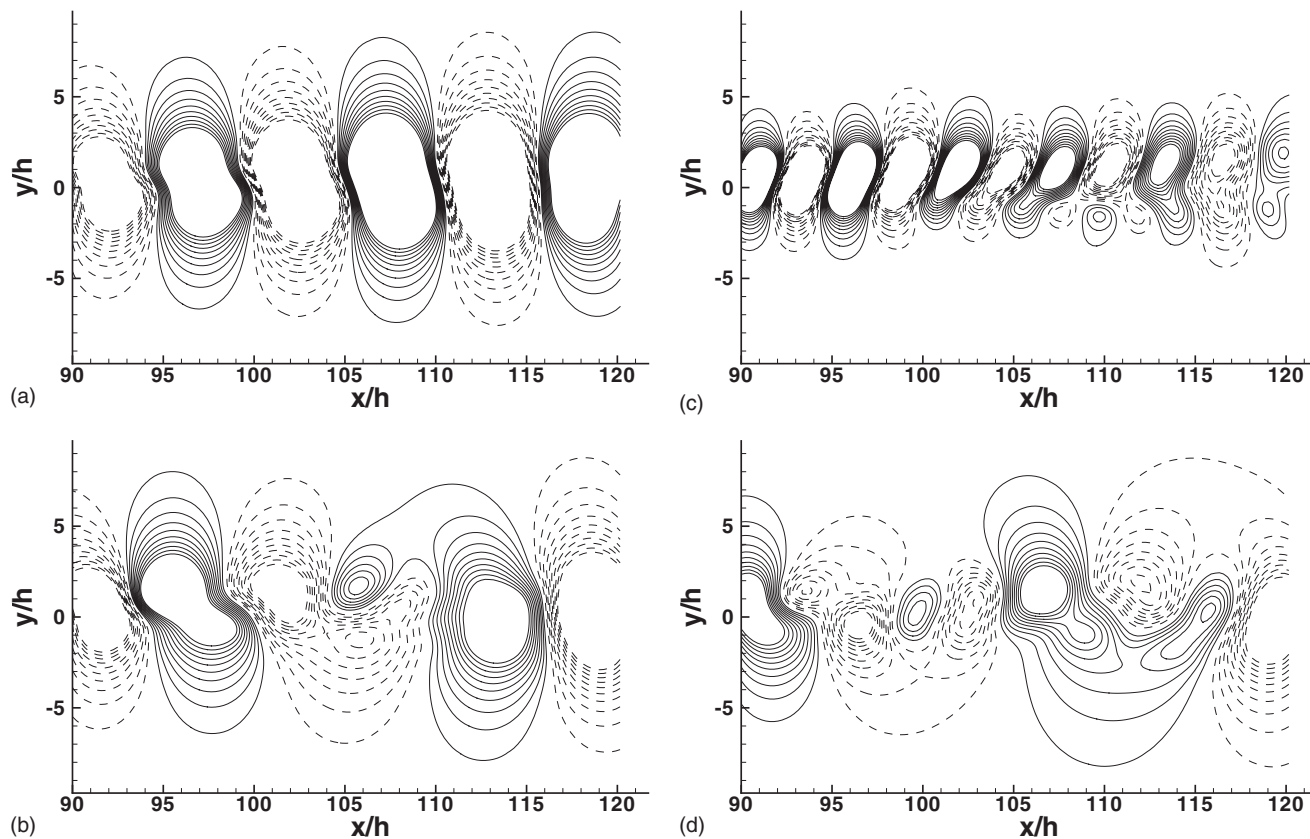
FIG. 15. Isocontours of the transverse POD component ξ_2^q for the ITE case, for $q=1$ (a), 3 (c), 5 (b), and 7 (d).
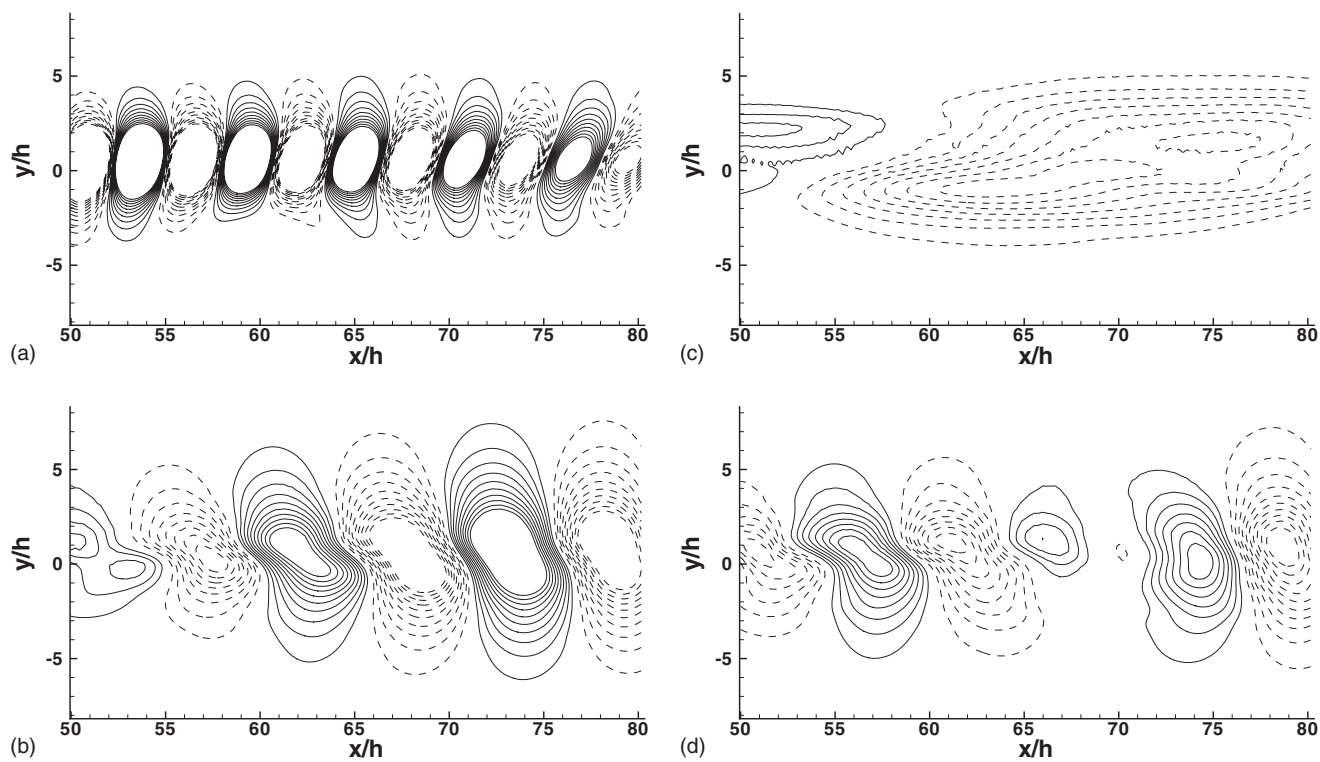

FIG. 16. Isocontours of the transverse POD component ξ_2^q for the BTE case, for $q=1$ (a), 3 (c), 5 (b), and 7 (d).
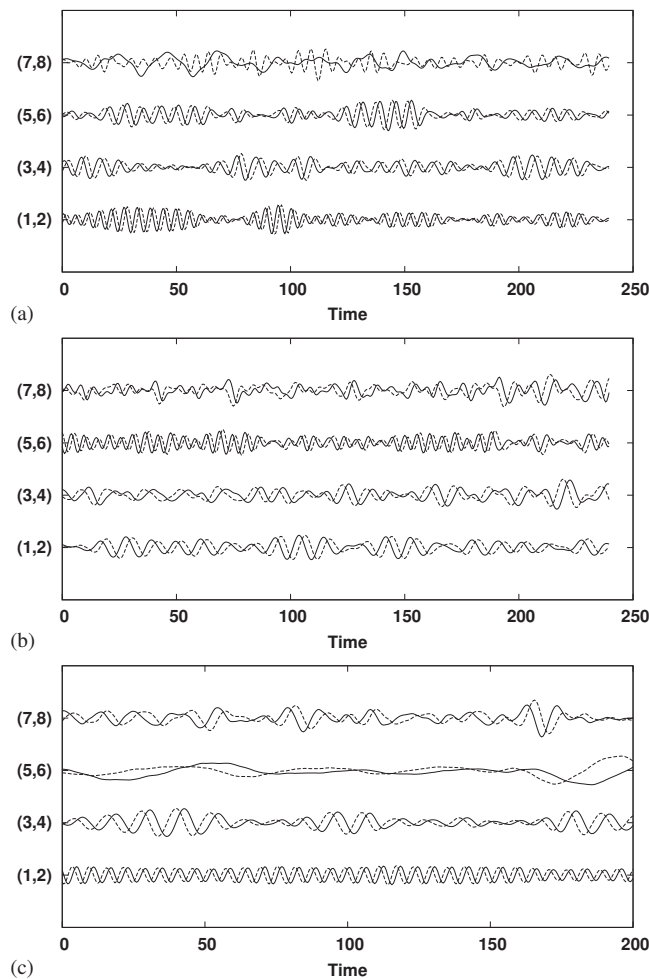
FIG. 17. Time evolution of the random coefficients $a^n(t)$ for each case: (a) TTE, (b) ITE, and (b) BTE.

even at the end of the computational domain. The dynamic is still almost harmonic [mode pair (1,2)], as shown in Fig. 17(b), and mode degeneration of those modes (pairing) is observed for the mode pair (3,4). The confirmation that pairing occurs for the ITE case in the near trailing-edge region explains the relative similarity observed on the growth rate (growth rate between 0.34λ and 0.38λ) at the end of the computational domain (Fig. 4) between all the three cases.

V. CONCLUSION

Instantaneous, statistical, and POD results are presented in this paper in order to explain the downstream-shape effects of a splitter plate on spatially developing mixing layer. DNS of spatially evolving mixing layer has been carried out with a thick trailing edge inside the computational domain, through the use of an IBM. Three different geometries have been studied, leading to three different flow dynamics. It is shown that the TTE case leads to a conventional mixing-layer evolution with no significant effects of the wake component introduced by the trailing edge. Indeed, due to the weak intensity of the near trailing-edge wake component, it can be considered that the turbulent state, with helicoidal pairing observed downstream the splitter plate, has "forgotten" the generation process. The only difference between

these simulations and previous reference results in literature concerns a slight overestimation of the spatial growth rate of the vorticity thickness. Again, it is important to notice that a thick splitter plate has been taken into account in the flow which could have an impact on the downstream flow dynamic, as already suggest in Ref. 9.

In contrast, for the BTE case, wakelike structures dominate in the first part of the flow, thus inhibiting the pairing process and its associated contribution to the mixing-layer growth. However, at the end of the computational domain, a more conventional mixing-layer dynamic can be observed with pairing and with a similar evolution for the vorticity thickness by comparison with the TTE case. The wake and mixing-layer components are both excited in the first part of the flow leading in return to strong and numerous streamwise vortices. However, the overestimation of the vorticity thickness growth is found to be more marked in this case, confirming the key role of the wake effect in such hybrid wake-/mixing-layer flows.

The ITE case which was supposed to be an intermediate case between the TTE and the BTE cases, with a smallest thickness for the trailing-edge end, finally gave the more surprising results. The elongated recirculation region observed just downstream the trailing edge leads to an inhibition of the 3D motions for a large part of the computational domain with the presence of large spanwise structures. Further downstream, the flow finally becomes more 3D and the main features of a transitional mixing layer can be observed. For this flow, the wake effect plays a fundamental role in the spatial development of the mixing layer, confirming the dependence on the inflow (generation) conditions.

The present study provides some useful information about the influence of a thick trailing edge on the dominance of spanwise coherent structures (overestimation of the two dimensionality of the flow) in the spatial development of a mixing layer, as previously observed in the experiments in Ref. 8.

Finally, it seems reasonable to hope that better quantitative DNS/LES predictions with experiments could be obtained by increasing drastically the Reynolds number and by improving the method for inflow condition generation, with a similar recycling technique used in Ref. 7 to obtain realistic turbulent data at the inlet of the computational domain.

ACKNOWLEDGMENTS

[1]J.-M. Chomaz, "Global instabilities in spatially developing flows: Non-normality and nonlinearity," Annu. Rev. Fluid Mech. **37**, 357 (2005).
[2]P. Huerre and P. A. Monkewitz, "Local and global instabilities in spatially developing flows," Annu. Rev. Fluid Mech. **22**, 473 (1990).
[3]W. K. George, "The self-preservation of turbulent flows and its relation to initial conditions and coherent structures," in *Advances in Turbulence*, edited by W. K. George and R. Arndt (Hemisphere, New York, 1989), pp. 39–73.
[4]M. Lesieur, *Turbulence in Fluids*, 4th ed. (Springer, New York, 2008).

[5] J. Mathew, I. Mahle, and R. Friedrich, "Effects of compressibility and heat release on entrainment processes in mixing layers," J. Turbul. **9**, 14 (2009).

[6] M. Rogers and R. Moser, "Direct simulation of a self-similar turbulent mixing layer," Phys. Fluids **6**, 903 (1994).

[7] N. D. Sandham and R. D. Sandberg, "Direct numerical simulation of the early development of a turbulent mixing layer downstream of a splitter plate," J. Turbul. **10**, 1 (2009).

[8] G. Brown and A. Roshko, "On density effects and large structure in turbulent mixing layers," J. Fluid Mech. **64**, 775 (1974).

[9] R. D. Metha, "Effect of velocity ratio on plane mixing layer development: Influence of the splitter plate wake," Exp. Fluids **10**, 194 (1991).

[10] P. Comte, J. H. Silvestrini, and P. Bégou, "Streamwise vortices in large-eddy simulations of mixing layers," Eur. J. Mech. B/Fluids **17**, 615 (1998).

[11] Y. Wang, M. Tanahashia, and T. Miyauch, "Coherent fine scale eddies in turbulence transition of spatially-developing mixing layer," Int. J. Heat Fluid Flow **28**, 1280 (2007).

[12] C. Braud, D. Heitz, G. Arroyo, L. Perret, J. Delville, and J.-P. Bonnet, "Low-dimensional analysis, using POD, for two mixing layer-wake interactions," Int. J. Heat Fluid Flow **25**, 351 (2004).

[13] S. Laizet and E. Lamballais, "Direct-numerical simulation of the splitting-plate downstream-shape influence upon a mixing layer," C. R. Acad. Sci., Ser. IIb: Mec., Phys., Chim., Astron. **334**, 454 (2006).

[14] L. Perret, J. Delville, and J.-P. Bonnet, "Investigation of the large scale structures in the turbulent mixing layer downstream a thick plate," Proceedings of the Third International Symposium on Turbulence and Shear Flow Phenomena, Sendai, Japan, 2003.

[15] D. Wallace and L. G. Redekopp, "Linear instability characteristics of wake-shear layers," Phys. Fluids A **4**, 189 (1992).

[16] D. A. Hammond and L. G. Redekopp, "Global dynamics of symmetric and asymmetric wakes," J. Fluid Mech. **331**, 231 (1997).

[17] B. Dziomba and H. E. Fiedler, "Effect of initial conditions on two-dimensional free shear layers," J. Fluid Mech. **152**, 419 (1985).

[18] S. Laizet and J. C. Vassilicos, "Multiscale generation of turbulence," Journal of Multiscale Modelling **1**, 177 (2009).

[19] E. Lamballais, J. Silvestrini, and S. Laizet, "Direct numerical simulation of a separation bubble on a rounded finite-width leading edge," Int. J. Heat Fluid Flow **29**, 612 (2008).

[20] E. Laurendeau, P. Jordan, J. P. Bonnet, J. Delville, P. Parnaudeau, and E. Lamballais, "Subsonic jet noise reduction by fluidic control: The interaction region and the global effect," Phys. Fluids **20**, 101519 (2008).

[21] P. Parnaudeau, J. Carlier, D. Heitz, and E. Lamballais, "Experimental and numerical studies of the flow over a circular cylinder at Reynolds number 3900," Phys. Fluids **20**, 085101 (2008).

[22] S. Laizet and E. Lamballais, "Direct numerical simulation of a spatially evolving flow from an asymmetric wake to a mixing layer," *Direct and Large-Eddy Simulation VI* (Springer, Poitiers, 2006).

[23] S. Laizet and E. Lamballais, "High-order compact schemes for incompressible flows: A simple and efficient method with quasi-spectral accuracy," J. Comput. Phys. **228**, 5989 (2009).

[24] P. Parnaudeau, E. Lamballais, D. Heitz, and J. H. Silvestrini, "Combination of the immersed boundary method with compact schemes for DNS of flows in complex geometry," *Direct and Large-Eddy Simulation V* (Springer, Munich, 2003).

[25] P. Holmes, J. L. Lumley, and G. Berkooz, *Turbulence, Coherent Structures, Dynamical Systems and Symmetry* (Cambridge University Press, Cambridge, 1996).

[26] J. Delville, "Characterization of the organization in shear layers via the proper orthogonal decomposition," Appl. Sci. Res. **53**, 263 (1994).

[27] L. Sirovich, "Turbulence and the dynamics of coherent structures. Part 1: Coherent structures," Q. J. Mech. Appl. Math. **45**, 561 (1987).

[28] M. Rajaee, S. K. F. Karlsson, and L. Sirovich, "Low-dimensional description of free-shear-flow coherent structures and their dynamical behaviour," J. Fluid Mech. **258**, 1 (1994).

[29] L. Sirovich, K. S. Ball, and L. R. Keefe, "Plane waves and structures in turbulence channel flow," Phys. Fluids A **2**, 2217 (1990).

[30] F. K. Browand and T. R. Troutt, "A note on spanwise structure in the two-dimensional mixing layer," J. Fluid Mech. **93**, 325 (1980).

[31] P. Comte, M. Lesieur, and E. Lamballais, "Large- and small-scale stirring of vorticity and a passive scalar in a 3-D temporal mixing layer," Phys. Fluids A **4**, 2761 (1992).